Chapter 4

Functionalized polyurethane composite gel electrolyte with cosensitized photoanode for higher solar cell efficiency using a passivation layer

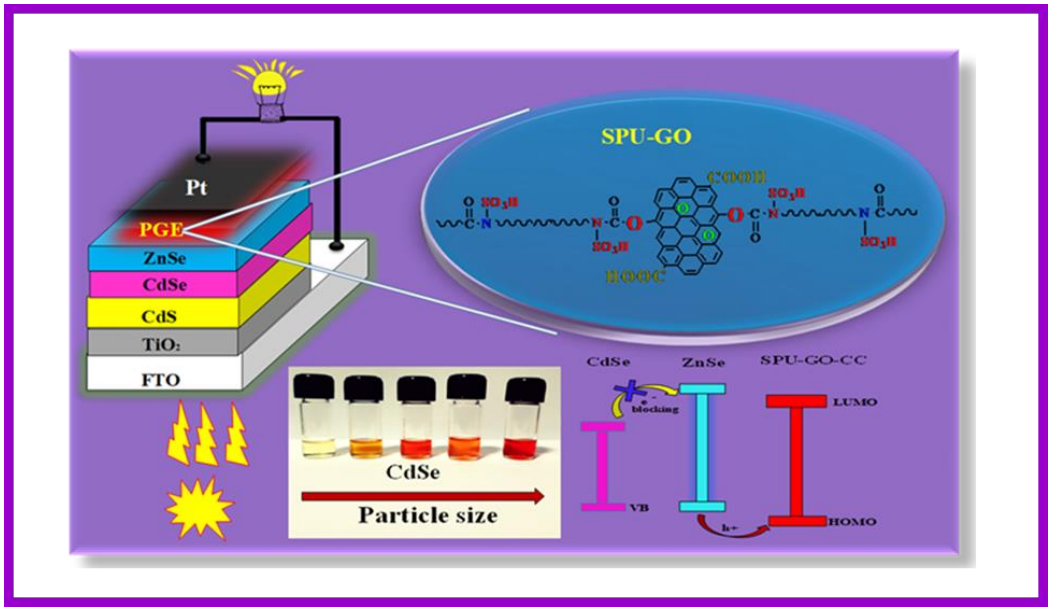

Nanoscale Advances. (2022); 4: 1199-1212

4.1 Introduction

Quantum dot solar cells have attracted attention in the modern era because of their low production cost, easy fabrication process and acceptable power conversion efficiency.[134,135] The inorganic QDs have lot more advantages as compared to dye molecules: (1) high extinction coefficient; (2) generation of multiple excitons through single-photon absorption; (3) tunable band gap; and (4) high photostability corresponding to water and oxygen.[136,137] The maximum theoretical power conversion efficiency of these devices is in order of 44%.[138] The surface passivation layer usually enhance the performance of QDSSCs, and this layer can form a uniform barrier layer to separate the photoanode with QDs and electrolytes as well as repair the surface defects of the QDs.[139,140] Well-designed passivation can reduce the electron recombination effectively and the layer promotes the separation process of electrons and holes.[141] The higher value of the conduction band edge of ZnS as compared to that of CdS/CdSe helps inhibit the transfer of electrons from the conduction band of QDs to LUMO levels of the electrolytes, and hence, usually used as a passivation layer. ZnSe is one of the suitable inorganic passivation materials to form a type of core–shell structure for CdS/CdSe QDs because of its suitable band structure and it has been widely used for QDSSC passivation.[142] Huang et al. have demonstrated that type of band alignment would not only prevent electron back transfer to the electrolytes but may also facilitate the desired hole transport from the QDs to electrolytes because both Ecb and Evb of ZnSe are higher than those of CdS/CdSe QDs.[138,143] However, ZnSe with a wide band gap and desirable electronic structure does not allow absorption in the long-wavelength regions.[142,144] The electrolytes have an important role in QDSSCs, which can complete the circuit by transferring of the hole to the counter electrode after receiving the holes from the valence band of QDs. The I^-/I_3 liquid electrolytes show the highest efficiency in DSSC, but these electrolytes cannot be effectively used in QDSSCs because of their corrosive character[145,146], sealing leakage and easy

evaporation. To overcome such issues, polymer electrolytes are the alternative materials of liquid electrolytes in QDSSCs. Polymer electrolytes were used to overcome problems such as corrosion of electrodes, leaking and sealing, shape flexibility, flammability issues and electrochemical stability. Polymer electrolytes are defined as a polymeric material complex with salt.[147,148] Polar functional groups in the main polymeric chain act as a medium to solvate the ionic species through intermolecular interactions and the ionic transport to occur by diffusion of the dissociated ions and their transport through the free volume of polymer matrix.[147,149] Polyurethane (PU) polymer matrix was functionalized to prepare polymer gel electrolytes, which were used to fabricated QDSSCs with co-sensitized CdS/CdSe photoanode to obtain 1.5% power conversion efficiency, and Kumar et al. used the functionalized thermoplastic polyurethane gel electrolytes in QDSSCs with TiO_2/CdS photoanode to achieve the PCE of 1.25%.[115] Recently, PU–GO nanocomposites have attracted the attention of many researchers, especially, as the mechanical and electrical properties of nanocomposites were significantly enhanced by adding only 1 wt.% of GO during the polymerization stage.[150,151] To enhance the properties of polymeric materials, composites are prepared by incorporating a small quantity of the filler in the polymer matrix. The polymer composites having low density and good thermal stability, better mechanical properties and higher electrical conductivity of polymer were increased by incorporation of the nanofiller in the polymer matrix.[152] The shifting of the peak position in spectroscopic measurements and lowering of melting temperatures are indicators of the extent of interaction. Our assumption is to develop GO-tagged polymer gel electrolytes as a better hole transport agent and the passivation layer was introduced to reduce the electron hole pair recombination which may enhance the device performance.

Here, in this work, an in-situ polymerization process was adopted to obtain the chemically tagged graphene oxide polyurethane polymer matrix (PU–GO), which is further functionalized to get a novel polymer gel electrolyte, i.e., the hole transport agent in QDSSCs. The prepared polymer gel electrolytes were used to fabricate QDSSCs with the cosensitized TiO2/CdS/CdSe photoelectrode. The optimum amount of the ZnSe passivation layer was deposited on the photoanode to reduce the electron–hole pair recombination as well as to increase the light-harvesting efficiency and also to enhance the photovoltaic performance of the fabricated QDSSCs. The underlying reasons are explored in detail.

4.2 Results and Discussion

4.2.1 Chemical Tagging of Graphene Oxide and its Interaction with Polymer Chain

The schematic reaction of the formation of GO-tagged polyurethane (PU–GO) in three stages of polymerization and subsequent functionalization of polyurethane polymer (SPU– GO) are shown in **Scheme 4.1**. ^{1}H NMR and FTIR spectroscopic measurements were used to confirm the chemical tagging of graphene oxide in polymer chains and its subsequent functionalization of the polymer (PU–GO). **Figure 4.1a** shows the ^{1}H NMR patterns of synthesized pure polyurethane (PU), GO-tagged polyurethane (PU–GO) and functionalized GO-tagged polyurethane (SPU–GO). Pure PU showed the peak at a chemical shift of δ = 8.54 ppm for >NH proton[153] while PU–GO showed two peaks for >N–H proton at 8.54 ppm (high intensity) and 8.45 ppm (low intensity) due to the presence of two types of >NH protons in the polymer chain with different chemical environments and the appearance of a new shielded peak at 8.45 ppm (absent in pure PU) is due to the interaction between graphene sheets (electrons rich) and >NH proton[154] in PU–GO polymer, confirming the chemical tagging of GO with the polymer (PU) chains. The functionalized polymer (SPU–GO)

shows a new strong peak at a chemical shift of δ = 8.48 ppm for –SO_3H proton and another two new peaks at δ = 1.9 and 1.6 ppm for –CH_2 protons[124,155] of the propane sultone group. This is to mention that these peaks are absent in pure PU and PU–GO polymer, which in turn, confirm the insertion of the sulfonate group in PU–GO polymer chains. In FTIR measurements, the prepolymer (PP) showed a characteristic peak at 3308 cm^{-1} due to the hydrogen-bonded >NH group[128] (stretching vibration) present in the prepolymer chain and the peak at 1778 cm^{-1} is responsible for the imide-carbonyl group[156] present in PP (**Figure 4.1b**).

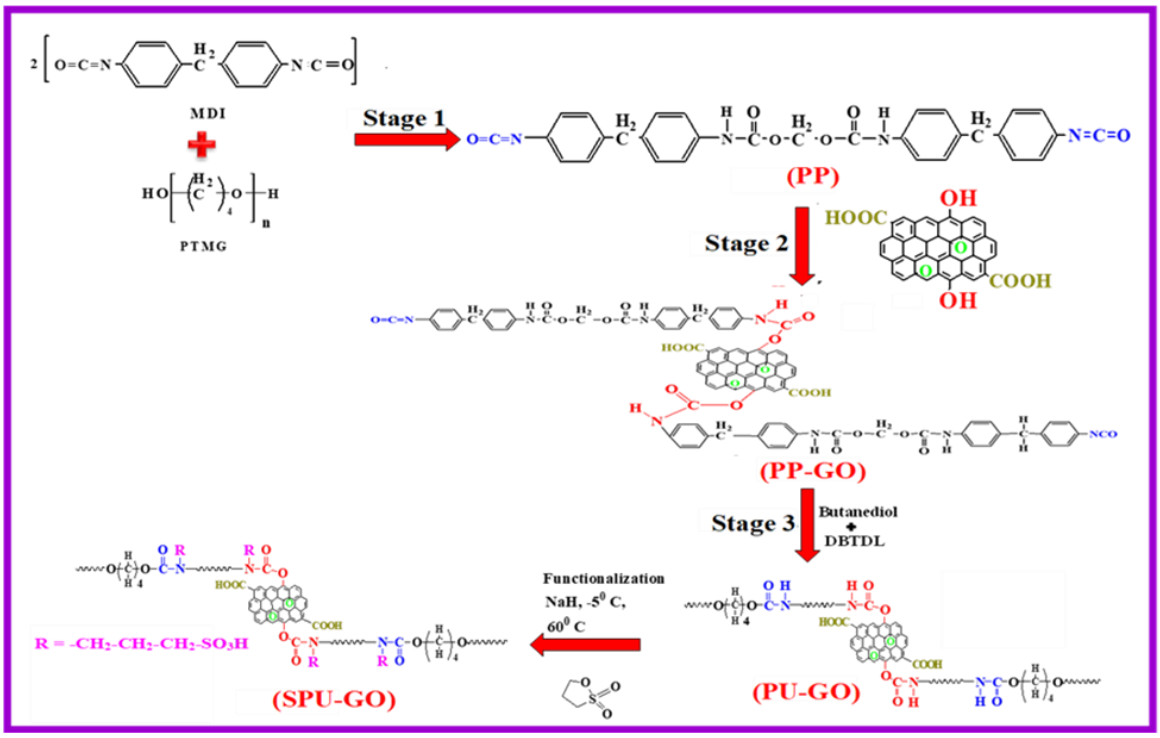

Scheme 4.1: Reaction scheme for the synthesis of GO tagged polyurethane (PU-GO) in three stages and its subsequent functionalization (SPU-GO).

After grafting of GO in prepolymer chains, the >NH peak is slightly shifted in GO-tagged prepolymer (PP–GO) due to the interaction between the graphene sheet and >NH bonds[154] and the GO-tagged polyurethane-extended polymer (PU–GO) shows a peak at 3305 cm^{-1} for the

hydrogen-bonded –NH group[128] present in the hard segment of polyurethane chains. The peak at 1778 cm^{-1} disappears[156] in PU–GO, suggesting the chain extension after the reaction with butanediol. Further, the hydrogen-bonded >NH peak becomes broad at 3413 cm^{-1} with the sulfonation of the PU–GO polymer[125] and SPU–GO exhibits a new strong peak at 1184 cm^{-1} due to the symmetrical stretching vibration of the S=O linkages after functionalization.

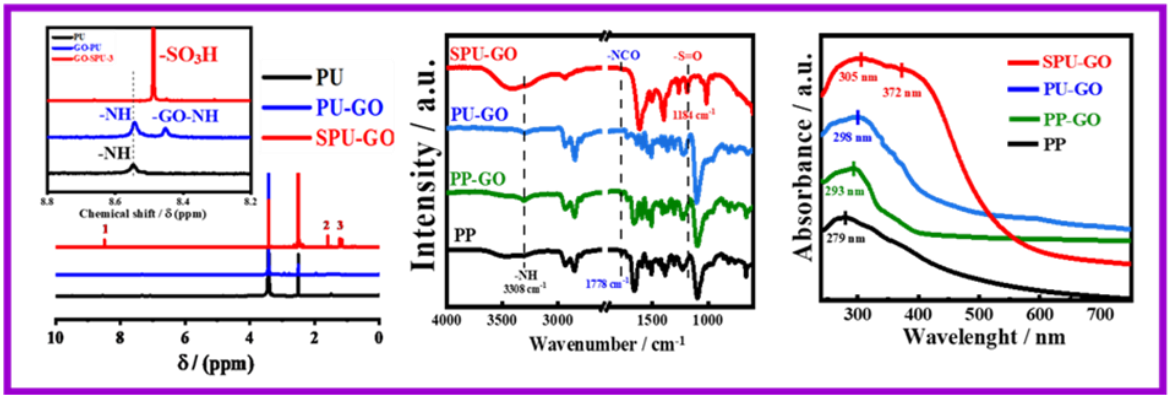

Figure 4.1: (a) ^{1}H NMR spectra of pure PU, PU-GO and functionalized polymer (SPU-GO), inset figure shows the magnified spectrum in the indicated zone; **(b)** FTIR spectra of PP, PP-GO, PU-GO and SPU-GO showing appearance of new peak and shifting of peak position; **(c)** UV-vis absorption spectra of PP, PP-GO, PU-GO and functionalized polymer (SPU-GO) showing shifting of peak position.

The UV-vis absorption spectroscopic measurement was performed to understand the interactive nature between graphene sheets and polymer chains**. Figure 4.1c** shows the UV-vis absorption patterns of PP, PP–GO, PU–GO and SPU–GO. The prominent peak in PP at 279 nm is due to n → p* transition[157] and it is red shifted to 293 nm in PP–GO due to the presence of the graphene sheet in the prepolymer chain. The peak position has further shifted to 298 nm in PU–GO after chain extension using butanediol. The SPU–GO polymer shows two broad peaks at 305 nm due to

n → π* transition of urethane linkage and another one is at 372 nm assigned as n → π* transition due to the presence of the polar sulfonate group in polymer chains. However, spectroscopic techniques clearly indicate the tagging of GO with the polyurethane chain and their subsequent sulphonation to convert into SPU–GO as ion conductive species.

4.2.2 Molar Mass and Thermal Properties

The molar masses of PP, PP–GO and PU–GO were determined by the gel permeation chromatography (GPC) measurements and are shown in **Figure 4.2a**. Molar masses (Mn) of PP, PP–GO and PU–GO are 5.2, 5.3 and 6.4 K, respectively, and the molar mass of PU– GO is higher than that of PP–GO after the addition of butanediol as the chain extender in the third stage of the polymerization reaction, which confirms the chain extension of the polymer. The molecular weight decreases after the functionalization of GO-tagged polyurethane and the molecular weight were found to 1.7 K as measured using GPC, presumably due to hydrolysis in the presence of acidic environment.

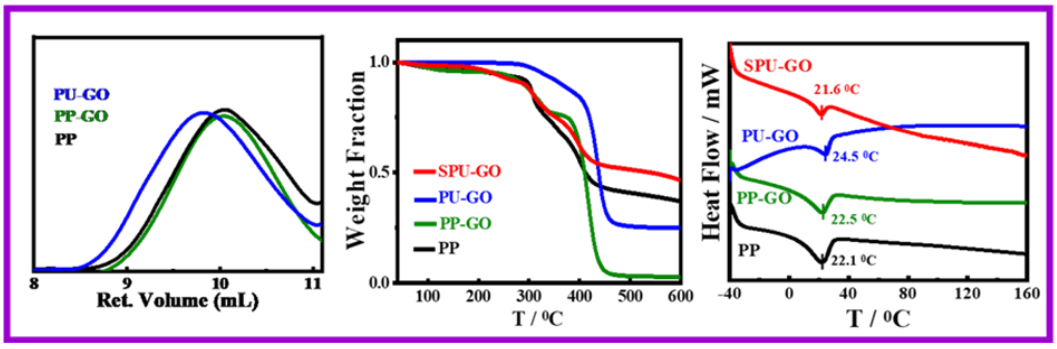

Figure 4.2: (a) DSC thermograms of PP, PP-GO, PU-GO and SPU-GO showing the melting temperatures; and **(b)** TGA thermograms of PP, PP-GO, PU-GO and SPU-GO showing relative thermal stability; **(c)** DSC thermograms of PP, PP–GO, PU–GO and SPU–GO showing the melting temperatures.

Thermal stabilities of the prepolymer, polymer and functionalized polymers were estimated using thermogravimetric analysis as shown in **Figure 4.2b**. Both the pure and functionalized polymers show two stages of degradation due to the hard and soft segments of the polymer chain and the functionalized polymer exhibits lower degradation as compared to pure polymer. The weight loss at a lower temperature is due to the degradation of the hard segment of the polymer chain and the soft segment is degraded at high temperature. The initial weight loss in SPU–GO is observed due to the hydrophilic nature of SPU–GO. The degradation temperatures were found to be 226 ^{0}C, 244 ^{0}C, 327 ^{0}C and 228 ^{0}C for PP, PP–GO, PU–GO and SPU–GO, respectively. The presence of graphene enhances thermal stability while sulphonation decreases the thermal stability a bit. This is to mention that the temperature corresponding to 5% weight loss is considered as the degradation temperature. However, the functionalized polymer was thermally stable up to 200 ^{0}C and thereby suitable for its application in solar cells. Differential scanning calorimetric measurements were used to analyze the melting behavior of specimens, as shown in **Figure 4.2c**. The melting temperature of PP was 22.1 ^{0}C and the presence of graphene oxide in the prepolymer enhances the crystalline nature of PP–GO, resulting in an increase in its melting temperature to 22.5 ^{0}C. The chain extension with butanediol in PP–GO further increases the melting temperature to 24.5 ^{0}C. The functionalization of the polymer in SPU–GO showed a melting temperature of 21.6 ^{0}C. The melting temperatures corresponding to the sot segment zone and crystallization of the soft segment were facilitated in the presence of graphene, acting as heterogeneous nucleation sites. The heat of fusion values was calculated as 25, 26.5, 27.9 and 6.3 J g^{-1} for PP, PP– GO, PU–GO and SPU–GO, respectively. The functionalization in SPU–GO reduces the crystallinity, both in terms of melting temperature and heat of fusion, predominantly due to the presence of sulphonate groups, which inhibits the main chain to fit into the crystalline lattice. Further, intermolecular interaction

enhances in the presence of the sulphonate group in SPU–GO, which causes lowering of melting and heat of fusion as compared to PU–GO. However, the small increase in heat of fusion along with the temperature is noticed in the presence of graphene in PP–GO and PU–GO suggesting enhanced heterogeneous nucleation.

4.2.3 Electrochemical Response of GO-Tagged Polyurethane Ionomer

The lower resistance of electrolytes is responsible for the better performance of solar cell devices. The prepared gel polymer electrolytes having low resistance with good ionic conductivity may facilitate better transportation of the holes in the operational mode of the devices. Electrochemical impedance spectrometry (EIS) measurements were used to calculate the ionic conductivity of the polymers. The Nyquist plots were used to measure the polarizing resistance of the polymers using the fit and simulation method **(Figure 4.3a)**. The resistance of PP was found to be 6.81×10^{-8} Ω and the introduction of the graphene sheet in the polymer chain reduces the resistance of PP–GO to 5.67×10^{-6} Ω due to the presence of graphene sheets, which helped in better transportation of the charge. The resistance was further decreased to 7.25×10^{-5} Ω in the extended polymer (PU–GO). The attachment of the sulfonate group (ionic moiety) in the main chain in SPU–GO exhibited the resistance of 6.25×10^{-2} Ω, and the incorporation of 0.052 wt.% of the conductive carbon (CC) to the prepared composite (SPU–GO–CC) caused a further decrease in the resistance to 5.28×10^{-2} Ω. The corresponding conductivities are presented in **Table 4.1.** However, the functionalized polymer (SPU–GO) and its composite (SPU– GO–CC) exhibited ionic conductivities in the range

of semiconductors (2.98×10^{-4} and 1.07×10^{-3} S cm^{-1}, respectively), hence, they were found suitable for solar cell device fabrication.

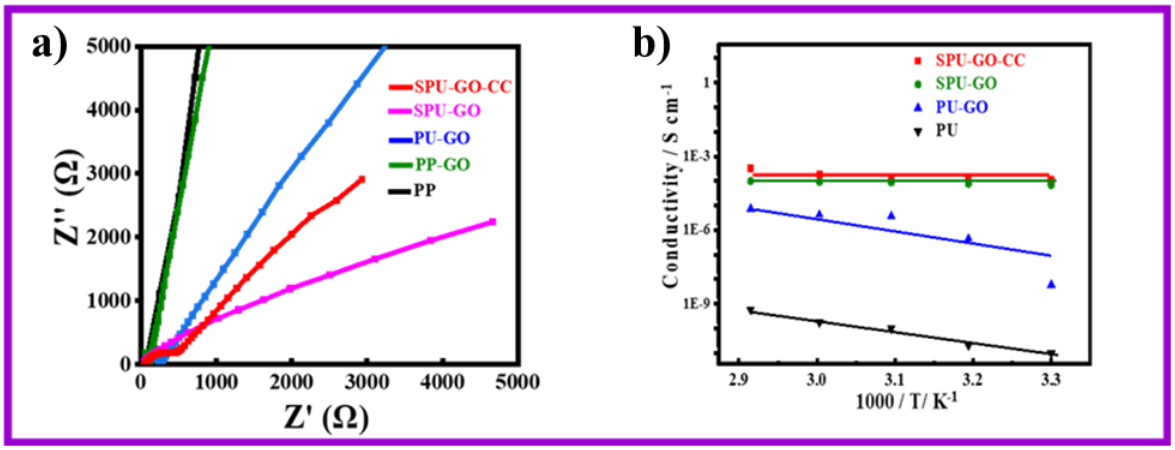

Figure 4.3: (a) Nyquist plots for the indicated pure and functionalized PUs; **(b)** Arrhenius plots of the pure and indicated functionalized polymers.

The specimens were sandwiched between two titanium electrodes and EIS data were recorded at different temperatures and Arrhenius behavior of polyurethane, PU–GO, SPU–GO and SPU–GO–CC were plotted/fitted using **eqn (2.7.1)** as shown in **Figure 4.3b**. The activation energies were calculated from the respective slopes of Arrhenius plots. The calculated values of activation energy from the Arrhenius plots were found to be 113.3, 61.5, 9.5 and 9.2 kJ mol^{-1} for pure PU, PU–GO, SPU–GO and SPU–GO–CC, respectively. The reduction of activation energy is due to the presence of the sulphonate group in the main chain and a similar reduction process is reported in the literature using sulfonated PU (15 kJ mol^{-1}).[158] The lower activation energy for the functionalized polymer is helpful for greater conduction and is likely to be suitable as a gel electrolyte in solar cell applications. From the EIS measurement, it is clearly observed that the ionic conductivities increase by tagging GO, which is further enhanced through functionalization,

followed by the addition of conducting carbon. Cell durability plays an important role in fabricating the solar cell device, which depends on the developed materials used in the solar cell. The corrosive nature of the most active ingredients is responsible for the low life cycle of the device.

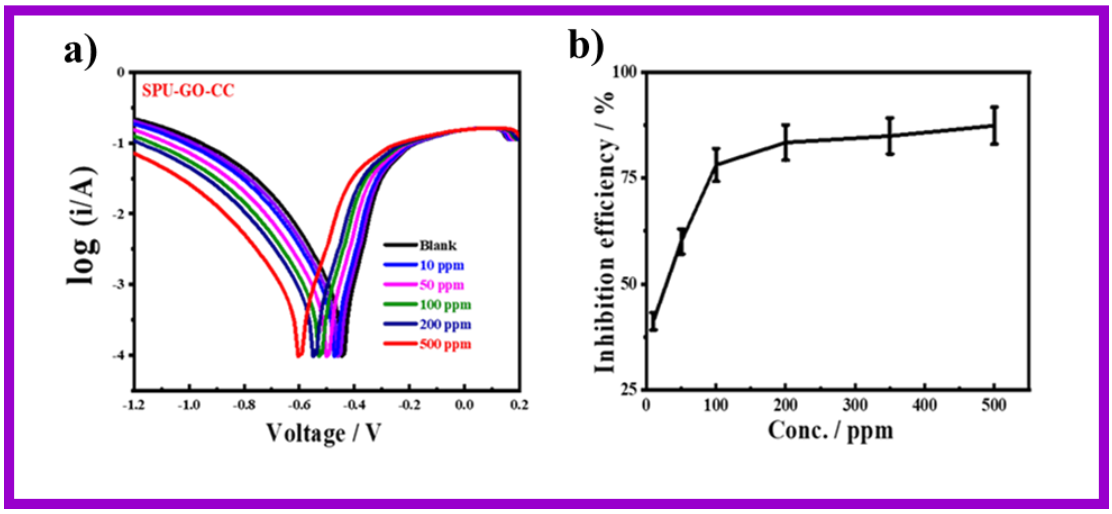

Figure 4.4: (a) Potentiodynamic polarization measurement of mild steel with and without the indicated inhibitors in 0.5 M H_2SO_4 solution; and **(b)** percentage inhibition efficiency as a function of inhibitor (SPU-GO-CC) concentration.

The corrosive nature/property was estimated using the potentiodynamic polarization measurement technique with a three-electrode setup assembled in a glass cell. Mild steel was used as a working electrode, Ag/AgCl as a reference electrode and platinum as a counter electrode. The dimensions of the working electrode were 3 × 1 × 0.1 cm^3 with an active area of 1 cm^2 and was dipped in 0.5 M H_2SO_4 acid solution. The corrosion potential (E_{corr}) and corrosion current densities (I_{corr}) were

calculated by extrapolating cathodic and anodic current–potential characteristics of the linear polarization Tafel plots up to their intersection point.

Table 4.1: The resistance and conductivities of various pure and functionalized polymer / composite.

S.N.	Sample	Resistance (Ω)	Conductivity (S/ cm)
1.	PP	6.81×10^{8}	2.10×10^{-11}
2.	PP-GO	5.28×10^{6}	1.02×10^{-9}
2.	PU-GO	7.25×10^{5}	5.08×10^{-7}
4.	SPU-GO	6.25×10^{2}	2.98×10^{-4}
5.	SPU-GO-CC	5.28×10^{2}	1.07×10^{-3}

The inhibitor efficiency was calculated from the measured Icorr values using the following equation;

$$IE\ \% = \frac{I^0_{corr} - I_{corr}}{I^0_{corr}} \quad \text{.....4.1}$$

where, I_{corr} and I^0_{corr} are current densities with and without the presence of inhibitors, respectively. The potentiodynamic polarization linear Tafel (I–V) plots are shown in **Figure 4.4a**. The I^0_{corr} and E^0_{corr} values were observed for the blank coupon (without inhibitor) and were found to be 6.445×10^{-6} A/cm^2 and -0.445 volt, respectively. The addition of 10 ppm concentration of SPU–GO–CC in the acidic solution decreases the corrosion current densities from 6.445×10^{-6} to 4.184×10^{-6} A/cm^2 and the corrosion potential was shifted from -0.445 to -0.459 V with inhibitor efficiency

(η) of 35 %. **Table 4.2** represents the variations of I_{corr}, E_{corr} and inhibitor efficiency (η) upon increasing the inhibitor concentration and the considerably high (87.40%) inhibitor efficiency (η) was observed using 500 ppm concentration of SPU–GO–CC inhibitor (**Figure 4.4b**). However, the developed system (SPU–GO–CC) exhibits anticorrosive properties with high inhibition efficiency. This is to mention that corrosion inhibition efficiency of 85 to 92 % is reported in the literature[112,124] using sulphonated polyurethane, similar results were obtained in this study.

Table 4.2: The corrosion current density, potential, corrosion rate density and percentage inhibition efficiency of functionalized polymer at different concentration

Inhibitor	Inhibitor concentration (ppm)	Corrosion potential (V)	Polarization resistance (Ω/cm^2)	Corrosion rate density (A/cm^2)	Inhibition efficiency (%)
Blank	—	**0.445**		**6.445**	—
SPU-GO-CC	**10**	**0.459**		**3.53**	**35.08**
SPU-GO-CC	**50**	**0.472**		**2.544**	**60.02**
SPU-GO-CC	**100**	**0.500**		**1.414**	**78.06**
SPU-GO-CC	**200**	**0.528**		**1.045**	**83.78**
SPU-GO-CC	**350**	**0.548**		**1.031**	**84.03**
SPU-GO-CC	**500**	**0.602**		**8.121**	**87.40**

4.3 Quantum Dots Synthesis, Morphology, and Optical Properties

The UV-vis absorption spectroscopic measurements on the synthesized CdS and CdSe QDs are shown in **Figure 4.5a.** The characteristic absorption peaks were observed in the visible region for both CdS and CdSe QDs at 492 and 541 nm, respectively.[115,125]

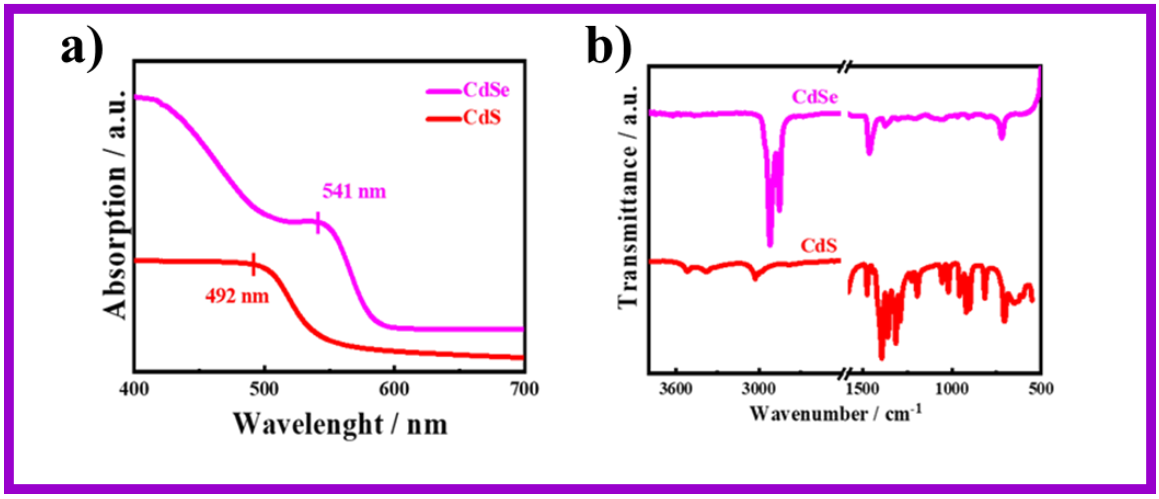

Figure 4.5: (a) UV-vis absorption spectra of CdS and CdSe showing the absorption peak; **(b)** FTIR spectra of synthesized CdS and CdSe QDs.

The capping of CdS with EDTA plays a significant role in the absorption behavior and the absorption band appears at 532 nm when prepared without any capping agent[159,160] (**Figure 4.6**). FTIR spectra of the prepared QDs are shown in **Figure 4.5b**. The peak at 3520 cm^{-1} appears for O–H stretching frequency of water molecules, which are absorbed on the CdS surface through hydrogen bonding[161] and the peaks at 705 cm^{-1} in CdS QD are due to the CH–stretching and bending mode of EDTA.[124,125] The CdSe QD shows intense peaks at 2919 and 2850 cm^{-1} due to antisymmetric and symmetric C-H stretching vibrations of the CH_2– group,[133] respectively, due to the capping agent of oleic acid. Other peaks at 1460 and 1373 cm^{-1} are due to antisymmetric

and symmetric vibration of the carboxylate anion[162] (COO^-), which confirms that the carboxylic group on the surface of CdSe QDs appears from the capping agent. This is to mention that the peak at 3483 cm^{-1} appears in CdS without any capping agent.[115]

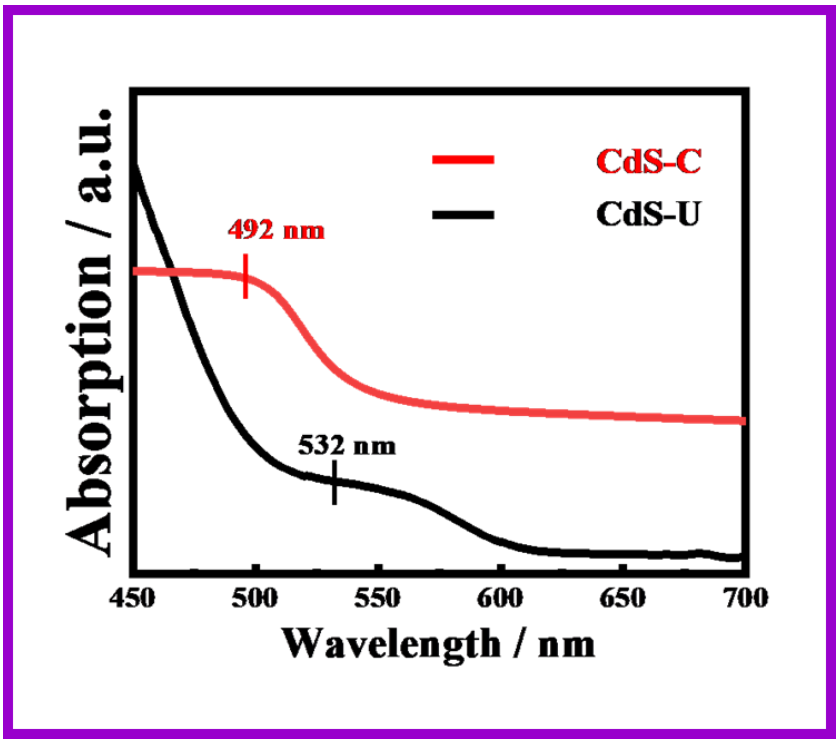

Figure 4.6: The UV-Vis absorption spectroscopy of EDTA capped and Uncapped of CdS QDs

The capping agent plays an important role in the size of the quantum dots and the average particle size of the synthesized QDs was determined using transmission electron microscopy (TEM) bright-field images and the average particle sizes were found to be 5 and 9 nm for CdS and CdSe QDs, respectively (**Figure 4.7 a and b**). This is to mention that a bigger particle dimension of 15 nm was measured for the quantum dots prepared without any capping agent.

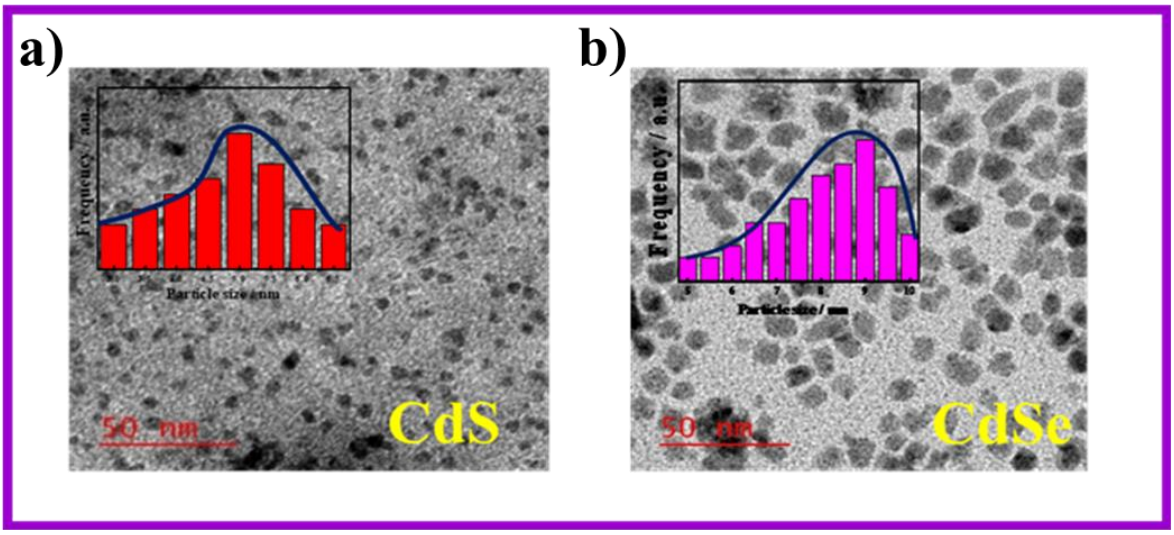

Figure 4.7: (a) TEM bright field image and particle distribution of CdS QDs; and **(b)** TEM bright field image and particle size distribution of CdSe QDs.

CdS and CdSe both are promising materials reported to have better performance in QDSSCs. CdS QDs have a higher band edge than that of TiO_2, which is more beneficial for the excited electron injection from CdS QDs, but the absorption range of CdS QDs are below the wavelength of 550 nm, whereas the absorption range of CdSe QDs may be extended to the 720 nm wavelength and the electron injection efficiency is less than that of CdS QDs, hence, to take both advantages of materials such as electron injection ability and light-harvesting capability of CdS, CdSe QDs were used to prepare the cosensitizer on TiO_2 film. So, the cosensitized photoanode is more effective than the single loaded either CdS or CdSe QDs.

4.4 Energy Levels Through Electrochemistry

The cyclic voltametric (CV) measurements are used to analyze the electrochemical response for electrode–electrolyte interfaces and to calculate the produced current after applying the voltage with a specific scan rate. In the redox reaction, the reduction of polymer chains becomes negatively charged while it is converted into positively charge species during oxidation.

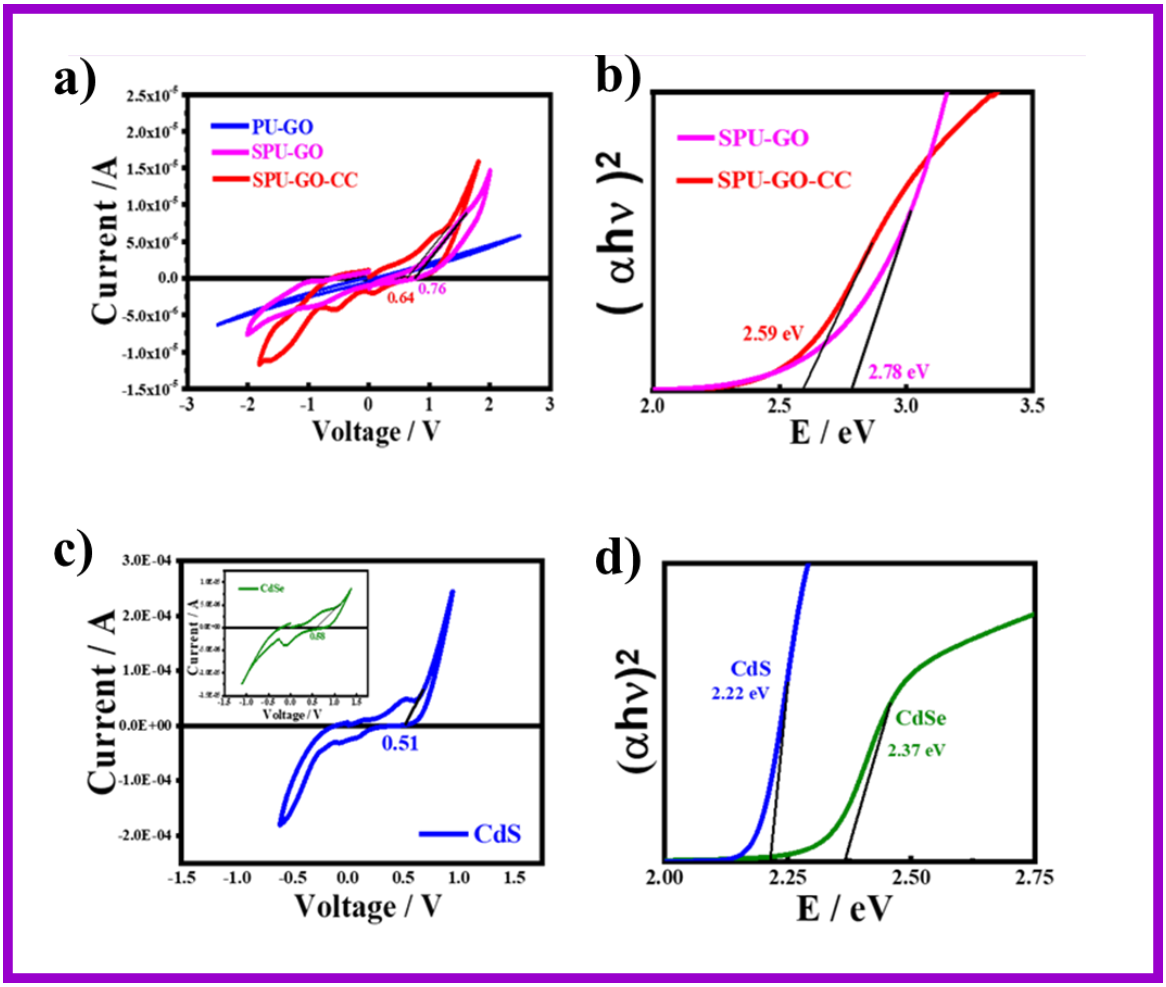

Figure 4.8: (a) CV voltammograms of PU–GO, SPU–GO and SPU–GO–CC polymer/composite; (b) optical band gap measurement of SPU–GO and SPU–GO–CC polymer/composite; (c) CV voltammograms of CdS and CdSe QDs; and (d) optical band gap measurements of CdS and CdSe QDs.

Figure 4.8a shows the current–potential curves of pure and functionalized polymers. The E_{OX} values for SPU– GO and SPU–GO–CC are 0.76 and 0.64 V, respectively. The E_{HOMO} for SPU–GO and SPU–GO–CC are found to be -5.16 and -5.04 eV, respectively, as calculated using **eqn. (2.5)**, and the optical band gap of SPU–GO and SPU–GO–CC are found to be 2.78 and 2.59 eV, respectively, using the Tauc's plots (**Figure 4.8b**). This is to mention that PU–GO does not exhibit any oxidation and reduction potential in the range studied here, as evident from the linear behavior of the current–voltage curve. The CV voltammograms of CdS and CdSe QDs are shown in **Figure 4.8c**. The E_{OX} value of CdS is calculated as 0.51 V and the E_{HOMO} and E_{LUMO} values are -4.91 and -2.69 eV, respectively, as calculated using the **eqn. (2.5) and (2.6).** Similarly, CV measurement of CdSe QDs is shown in **Figure 4.8c** (inset), and the E_{OX} value is found to be 0.58 V and E_{HOMO} and E_{LUMO} values are -4.98 and -2.61 eV, respectively (**Figure 4.8d**). The electrochemical properties of photoanode are changed with the layered patterns. The open-circuit voltage for TiO_2/CdS, TiO_2/CdSe, TiO_2/CdSe/CdS, TiO_2/CdS/ CdSe, and TiO_2/CdS/CdSe/ZnSe photoanodes had the values of 0.36, 0.21, 0.24, 0.54 and 0.73 volts, respectively, as observed through the EIS measurement; hence, the most suitable photoanode was found to be TiO_2/CdS/CdSe/ZnSe with the highest open-circuit voltage of 0.73 V and is used to fabricate the QDSSCs. The CV measurements used to calculate the HOMO and LUMO energy levels of the various functionalized polymer (SPU-GO-CC) materials are shown in **Figure 4.9**

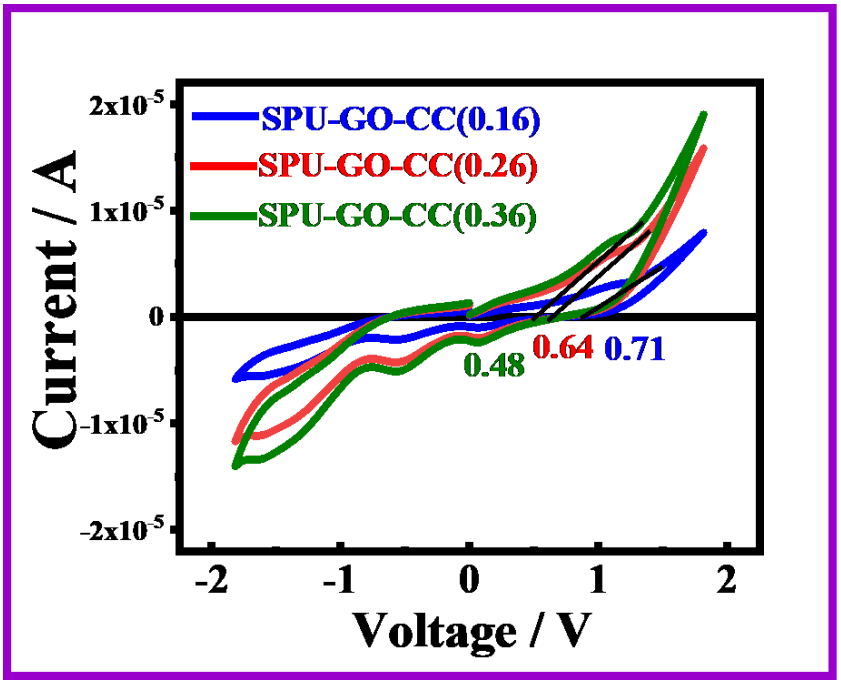

Figure 4.9: The CV measurement of functionalized polymer with varying content of conducting carbon additives.

4.5 Energy Diagram, Passivation Effect and Hole Transports Mechanism

The HOMO and LUMO energy levels of all polymers and QDs are combined to draw the energy profile diagrams, which are shown in the **Figure 4.10 (a-e)** to understand the suitable match of energy levels for better materials to fabricate solar cells devices. The optimized perfect match of the energy profile diagram of the functionalized polymer with CdS/CdSe QDs along with the respective electrodes is shown in **Figure 4.11a.**

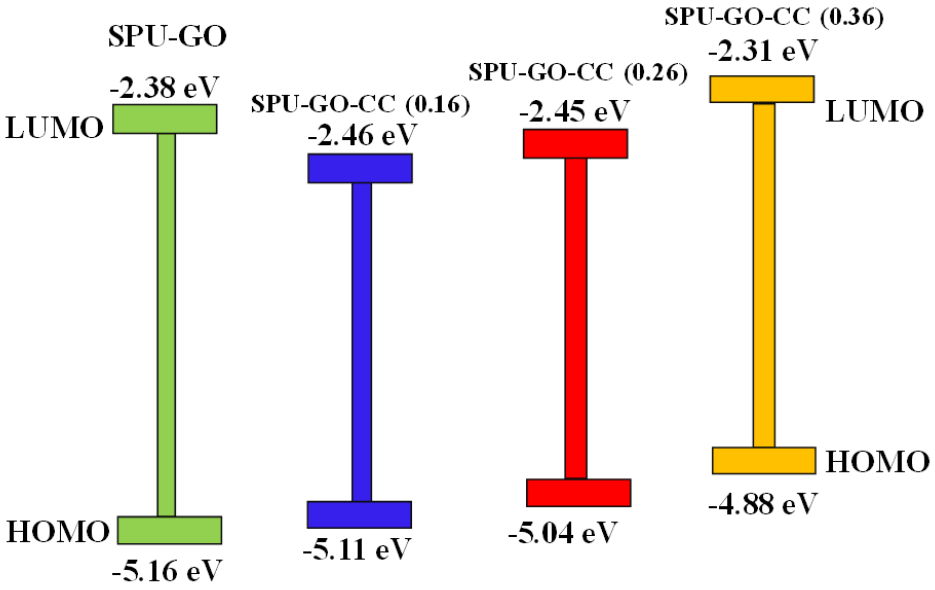

Figure 4.10: (a) The HOMO and LUMO energy levels of various functionalized polymers are used to draw the energy profile diagrams of functionalized polymers.

The hole transportation is faster from the conduction band of CdSe QDs to E_{HOMO} of SPU–GO–CC, as compared to the SPU–GO due to low energy gap/close proximity between VB of CdSe and E_{HOMO} of SPU–GO–CC as shown in **Figure 4.11b**. Hence, the functionalized composite SPU–GO–CC is a suitable material as a polymer gel electrolyte for the fabrication of solar cells. The hole transportation is faster from the conduction band of CdSe QDs to E_{HOMO} of SPU–GO–CC, as compared to the SPU–GO due to low energy gap/close proximity between VB of CdSe and E_{HOMO} of SPU–GO–CC as shown in **Figure 4.11b**. Hence, the functionalized composite SPU–GO–CC is a suitable material as a polymer gel electrolyte for the fabrication of solar cells.

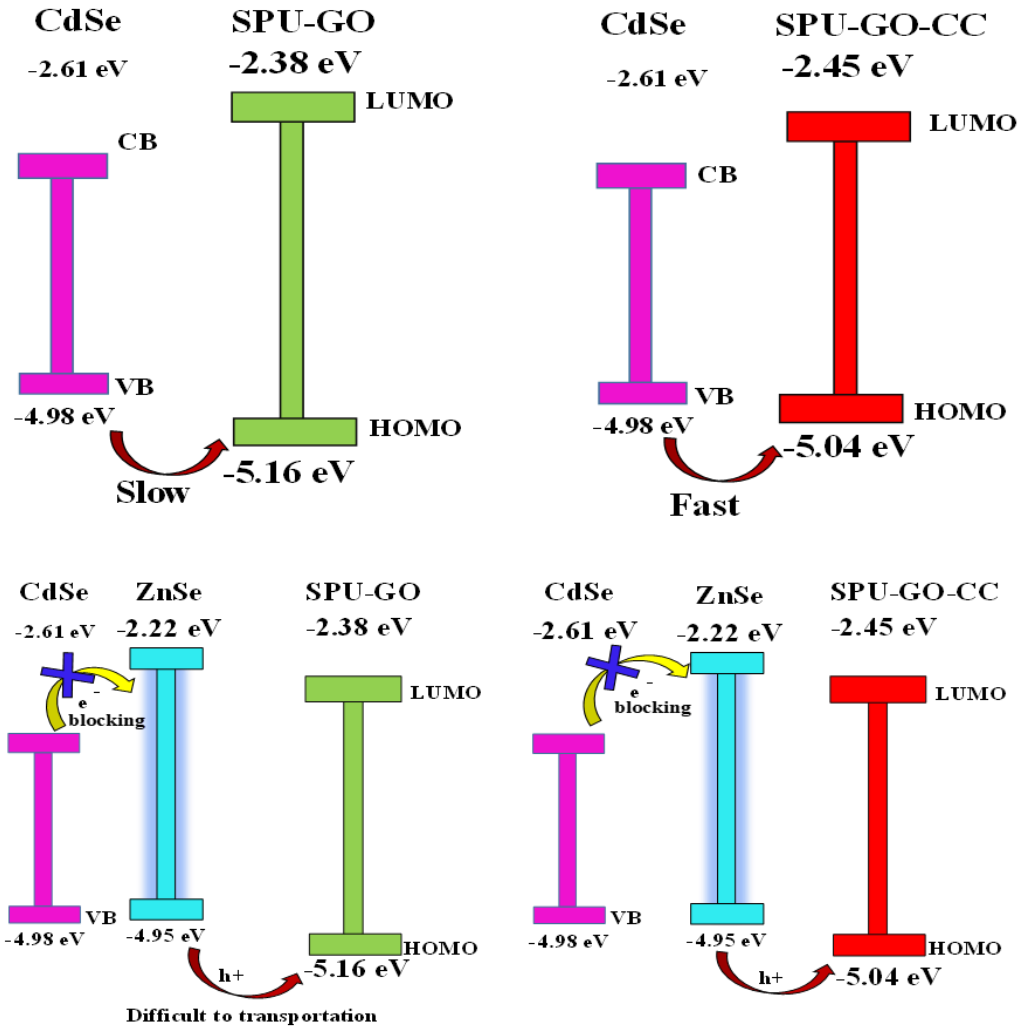

Figure 4.10: (b) The comparative band energy diagrams of functionalized polymer with and without passivation layer

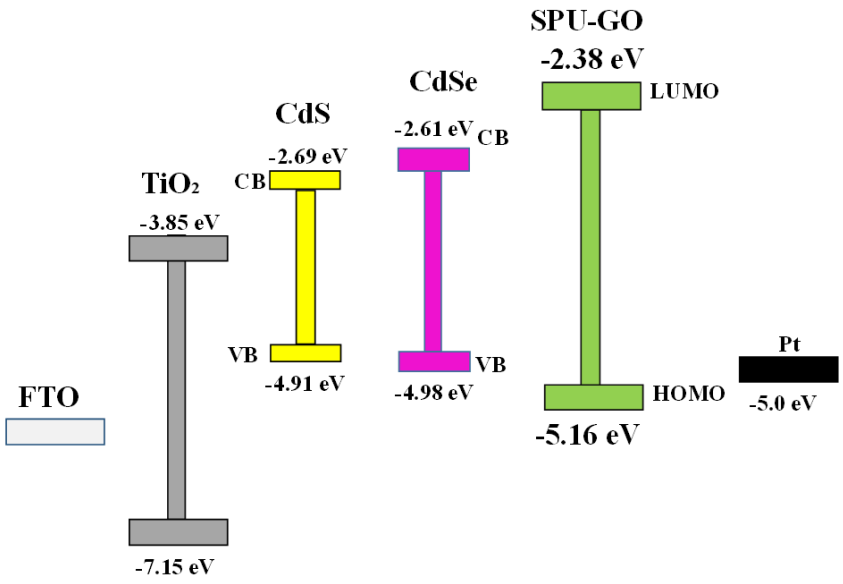

Figure 4.10: (c) The energy levels diagrams of SPU-GO polymers and QDs

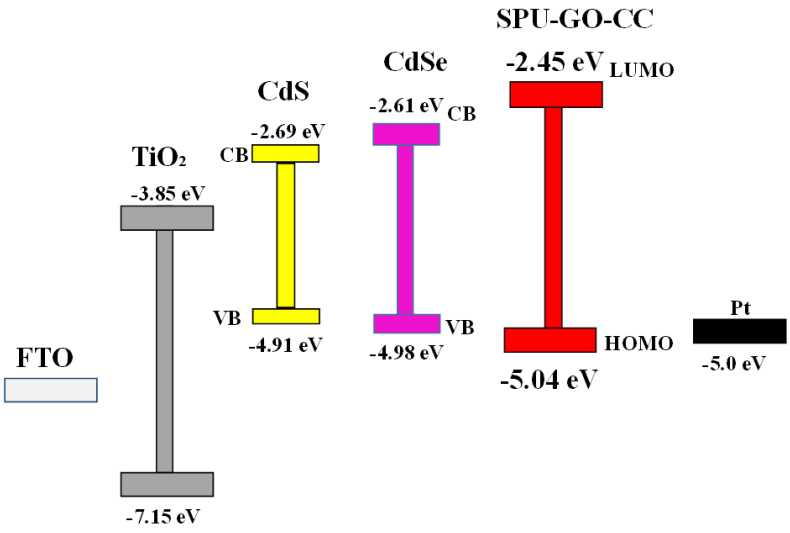

Figure 4.10: (d) The energy levels diagrams of SPU-GO-CC polymers and QDs

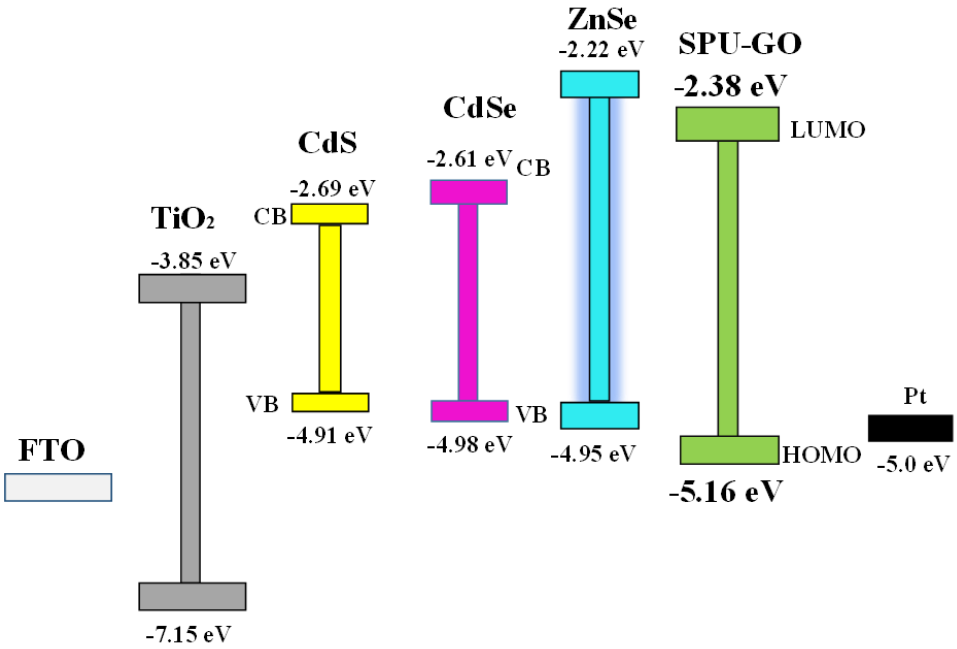

Figure 4.10: (e) The energy levels diagrams of SPU-GO-CC polymer and QDs with passivation layer.

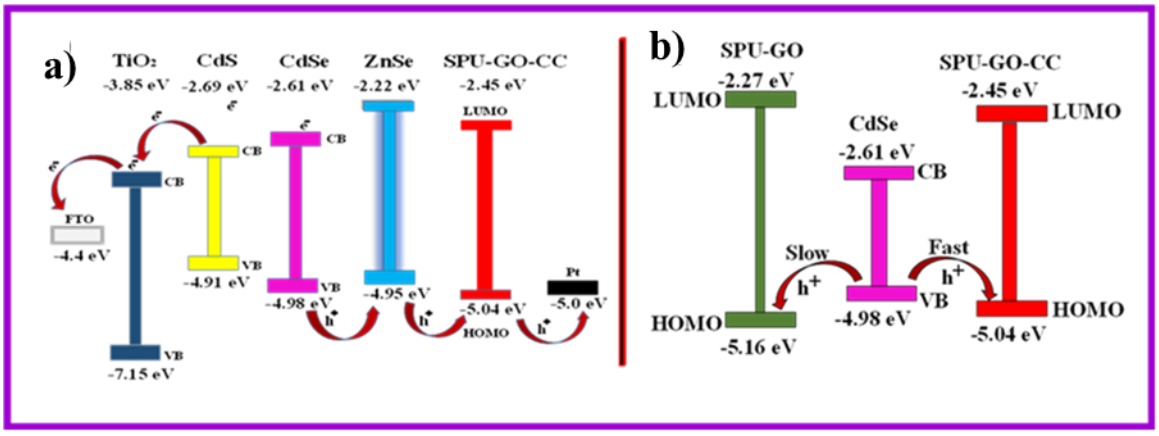

Figure 4.11: (a) Energy profile diagram of TiO_2, CdS and CdSe with SPU-GO-CC gel electrolyte; (b) comparison of energy level of the SPU-GO and SPU-GO-CC with CdSe QDs showing the transports behavior of holes.

4.6 Light-Harvesting Efficiency and Device Structure

It is essential to develop a greater light-harvesting material that eventually generates more excitons under the irradiation of sunlight. The light-harvesting efficiency (LHE) of TiO_2, TiO_2/ CdS, TiO_2/CdSe, and TiO_2/CdS/CdSe/ZnSe (ZnSe as the additional layer over the active materials/layer, acting as the passivation layer) is shown in **Figure 4.12 a.** Light-harvesting of the combined layers of CdS and CdSe exhibits a red shift in terms of light absorption compared to an individual later of either CdS or CdSe. Light-harvesting of TiO_2/CdS/CdSe/ZnSe is significantly higher compared to that without the passivation layer. Hence, the ZnSe passivation layer has enhanced the LHE, which can help in generating multiple excitons from the overall system. Another important role of the passivation layer is shown in the energy profile diagram, E_{HOMO}, E_{LUMO}, and optical band gap values of ZnSe are -4.95, -2.22 and 2.73 eV, respectively. Two SILAR cycles are used to deposit the passivation layer on QDs surface for the better performance of devices and can be attributed to higher intensity and greater red shift of light absorption in the 400–700 nm range and increases the electron concentration in the TiO_2 substrate, overall sensitized by the CdS/CdSe/ZnSe layer. The photoexcitation mechanism and the layered structure of the fabricated QDSSCs are shown in **Figure 4.12b**. After the absorption of a photon by CdSe QDs, the electron–hole pairs are generated and the electrons are easily transported from the valence band (VB) of CdSe to the CB of CdS through the CB of CdSe and the passivation layer of ZnSe facilitates the hole transportation from the VB of CdSe QDs to the HOMO level of SPU–GO–CC and prohibits the recombination of electron–hole pair, resulting in improved performance of QDSSC devices. Further, the ZnSe passivation layer prohibits the electron transport from the CB band of CdSe to the LUMO level of SPU– GO–CC.

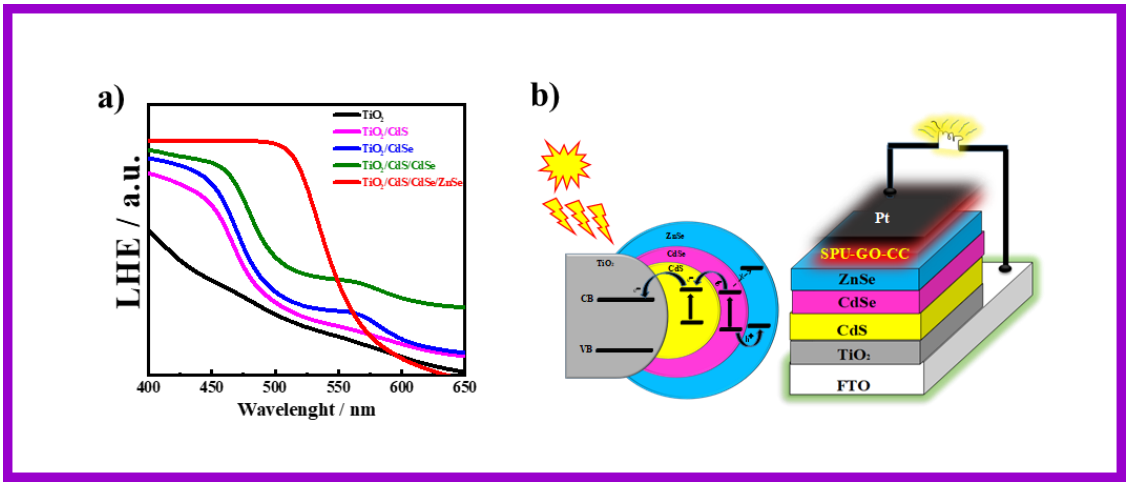

Figure 4.12: (a) Light harvesting efficiency of layer-by-layer deposition of QDs photoanodes FTO/TiO_2, FTO/TiO_2/CdS, FTO/TiO_2/CdS/CdSe and ZnSe passivation layer; and (b) Solar excitation mechanism and layered structure of fabricated QDSSCs.

The incorporation of the passivation layer between the hole transport layer material and TiO_2/CdS/CdSe cosensitized photoanode prohibits the electron–hole recombination because of the considerable energy-level difference between VB of CdSe QDs and ZnSe (0.39), which is higher, as compared to the LUMO level of the prepared composite polymer gel electrolytes and VB of CdSe (0.16). Hence, back electron transfer is difficult resulting in fewer electron–hole recombination, as compared to the system without any passivation layer. The introduction of ZnSe as the passivation layer also exhibited a considerable increment of absorbance and red shift in the literature.[143] However, the passivation layer facilitates hole transport while it prohibits electron transport to the gel electrolyte and ultimately suppresses the electron–hole pair recombination phenomena (usually responsible for low energy conversion efficiency).

4.7 Photovoltaic Performance of QDSSCs

The photocurrent–voltage (J–V) characteristic curves of the cosensitized TiO_2/CdS/CdSe photoanode using various polymer gel electrolytes with and without the ZnSe passivation layer under solar radiation (AM 1.5 G) with a light intensity of 100 $mWcm^{-2}$ are shown in **Figure 4.13a**. The cosensitized TiO_2/CdS/CdSe photoanode using the prepared polymer gel electrolytes (SPU–GO) showed the high fill factor (FF) value of 0.55 and the open-circuit voltage (V_{oc}) is 0.51 V but the photocurrent density observed is low J_{max} = 1.92 mA cm^{-2}, resulting in a low power conversion efficiency (PCE) of (η) = 0.51%, and hence, there is a need to improve the PCE. The power density– voltage curve is shown in **Figure 4.13b**, which represents the variation of the maximum power output (P_{max}) under solar radiation. The open-circuit voltage (V_{oc}), short circuit current density (J_{sc}), FF and PCE (η) of these cells with various assemblies are presented in **Table 4.3.** The (SPU–GO–CC) polymer gel electrolytes and cosensitized TiO_2/CdS/CdSe photoanode with two SILAR cycles of ZnSe passivation layer showed the highest PCE (η = 1.71%) with FF of 0.46 and open-circuit voltage (V_{oc}) of 0.73 V and short circuit current density (Jsc) of 5.09 mA cm^{-2} as compared to that without using any passivation layer. There are two optimization parameters behind the high performance of the fabricated device. One is the high conductivity of the prepared polymer gel electrolytes by tagging graphene oxide in the pure polymer chain and subsequent addition of the optimized amount of conductive carbon (0.052%) in the prepared gel electrolytes due to which the charge transportation phenomena become fast. Another important step is the incorporation of ZnSe as the passivation layer on the cosensitized photoanode, which acts as a blocking layer of electrons and reduces the recombination of electron–hole pairs.

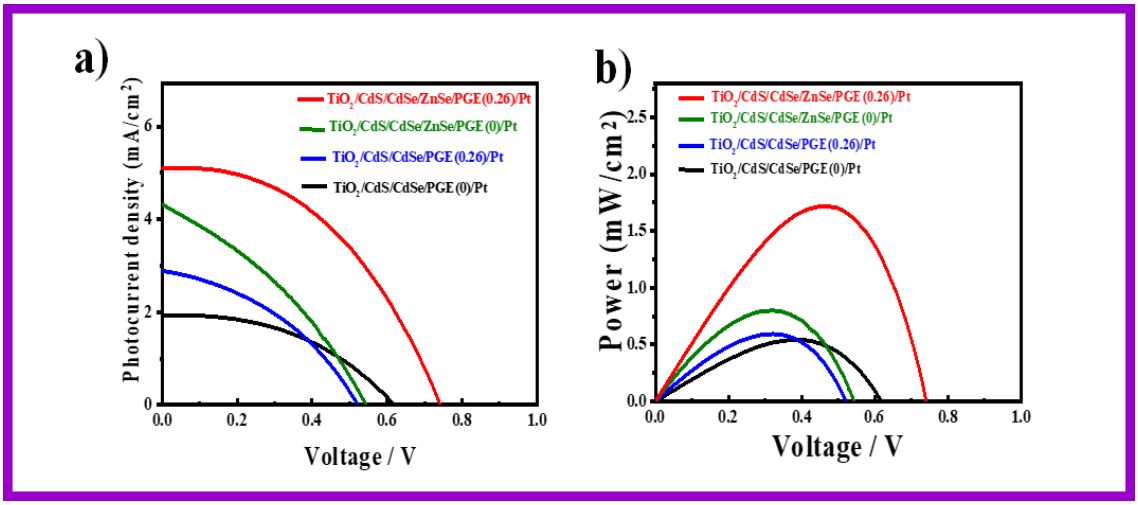

Figure 4.13: (a) *J-V* characteristics measurement to calculate the photocurrent density and open circuit voltage under 1-Sun illumination (100 mW/cm^2); and (b) power-voltage curve to calculate the power conversion efficiency (PCE) of the indicated QDSSCs.

The polymer gel electrolyte with 0.052 wt.% conductive carbon (SPU–GO–CC) was prepared and used in QDSSCs, which exhibits low electrical resistance and high electrical conductivity causing enhanced photocurrent density by 1.92 to 2.89 mA cm^{-2} and open-circuit voltage from 0.51 to 0.55 V while the fill factor of QDSSCs decreases from 0.55 to 0.38. The power conversion efficiency of the cell increases from η = 0.54 to 0.60 % of the QDSSCs due to the enhancement of the photocurrent density. The ZnSe passivation layer has been introduced between the cosensitized photoanode and polymer gel electrolytes, which plays an important role as an electron blocking layer (electron cannot pass onto gel electrolyte) while helping in charge transportation process of the hole transport from VB of CdSe to the HOMO level of the gel electrolyte through ZnSe layer because of the proximity of the energy level. Thereby, ZnSe acts as an effective passivation layer.

The performance of QDSSCs using the cosensitized TiO_2/ CdS/CdSe photoanode and polymer gel electrolyte (SPU–GO) with the ZnSe passivation layer achieved PCE of (η) = 0.81% and photocurrent density J_{max} of 4.32 mA cm^{-2}, open-circuit voltage V_{oc} of 0.61 V, while the fill factor (FF) becomes 0.31.

Table 4.3: Open-circuit voltage (Voc), short-circuit current density (Jsc), fill factor and power conversion efficiency, PCE (h) of various cells using the cosensitized photoanode and polymer gel electrolytes with and without the ZnSe passivation layer

Photoanode	**J_{max} (mA/cm^2)**	**V_{oc} (V)**	**Fill Factor**	**Efficiency**
TiO_2/CdS/CdSe[a]	**1.92**	**0.51**	**0.55**	**0.54**
TiO_2/CdS/CdSe[b]	**2.89**	**0.54**	**0.38**	**0.60**
TiO_2/CdS/CdSe/ZnSe[a]	**4.32**	**0.61**	**0.31**	**0.81**
TiO_2/CdS/CdSe/ZnSe[b]	**5.09**	**0.73**	**0.46**	**1.71**

[a] Device using SPU–GO as the electrolyte. [b] Device using SPU–GO–CC composite gel electrolyte.

The high photocurrent density J_{max} of 5.09 mA cm^{-2}, open-circuit voltage (V_{oc}) of 0.73 V with a significant fill factor (FF) 0.46 with PCE of the QDSSCs, (η) = 1.71% was obtained by using the cosensitized TiO_2/CdS/CdSe photoanode and polymer gel electrolytes SPU– GO–CC with the ZnSe passivation layer. The better performance of the QDSSCs is due to the high electrical conductivity of polymer electrolytes obtained by adding the optimized amount of conductive carbon, which improves the better charge transportation and passivation layer and, thereby, play

an important role, reducing the electron–hole recombination process and helping the charge (hole) transportation process between QDs and polymer gel electrolytes. This is to mention that negligible efficiency of 6.08×10^{-9} % was obtained using pure PU as the electrolyte gel from a poor J_{sc} of 5.2×10^{-6} mA cm^{-2}, while one order higher efficiency was achieved (8.79×10^{-8} %) by tagging the graphene moiety in PU (PU–GO as a gel electrolyte), which in turn indicates the superior effect of functionalization. However, a novel polymer gel electrolyte is developed by tagging graphene oxide in the main chain followed by further chain extension and functionalization. The use of ZnSe as a passivation layer is helpful to restrict the recombination of electron–hole pairs by stopping the electron flow from ZnSe (conduction band) to gel electrolyte (LUMO level). The addition of a minute quantity of conducting carbon significantly improves the power conversion efficiency through the higher conductivity of the system. In gist, superior gel electrolyte along with modified stacking layers of cosensitizer and passivation layer revealed a much-improved solar cell device.

4.8 Conclusion

Our strategy to synthesize the chemically tagged Graphene oxide with thermoplastic polyurethane and vary the chain lengths through chain extenders such as butanediol. Polyurethane was further functionalized by attaching the sulfonate group to the main chain. The confirmation of chemical tagging of GO was understood through ^{1}H NMR, FTIR and UV spectroscopic measurements. The presence of graphene sheets reduced the electrical resistance (increasing conduction) of PU thermoplastics. Further, the ionic polar moiety enhanced the conductivity of GO-tagged PU (SPU–GO) and a semiconducting (1.07×10^{-3} S cm^{-1}) and a suitable gel electrolyte is developed for QDSSCs. The HOMO and LUMO energy levels of the functionalized polymers, depending upon

the extent of functionalization's, were measured through cyclic voltametric measurements. Quantum dots, active materials like CdS and CdSe, were synthesized using suitable capping agents and their dimensions were measured through TEM bright-field images. The optical band gaps of the quantum dots were calculated using the light absorption measurements along with the relative light-harvesting efficiencies of individual and cosensitized systems. The electrical conductivity of functionalized polymer was increased by adding a minute quantity of conducting carbon (0.052%) and the HOMO / LUMO energy levels were optimized (close proximity) to the CB / VB of CdSe QDs. ZnSe has been used as a passivation layer, between the cosensitized photoanode and gel electrolytes, and the light harvesting efficiency was increased by depositing ZnSe on active materials. Finally, the solar cell devices were fabricated by using the cosensitized photoanode with the ZnSe passivation layer and functionalized polyurethane coupled with the conducting carbon (SPU–GO–CC) gel electrolyte to obtain a power conversion efficiency of 1.71%. The roles of conducting carbon and passivation were explored as increasing the level of conduction and blocking the charge carriers as required to enhance the ultimate efficiency by reducing the chances of electrons–hole pair recombination. The limitation of the experimental work is to fabricate and measure the device performance in inert atmosphere.